Supporting Information

Optimization of Electron Transfer Kinetics Between Photoanode and Biocathode for Enhanced Carbon-Neutral Pollutant Removal in Photocatalytic Fuel Cells

Xiaofei Gu [‡, a], Jianyu Han [‡, b, *], Zhi Wang [c], Yixin Hong [a], Tianyi Huang [a], Yafeng Wu [a], Yuanjian Zhang [a], Songqin Liu [a, *]

‡These two authors contributed equally to this work.

[a] *Jiangsu Engineering Laboratory of Smart Carbon-Rich Materials and Device, School of Chemistry and Chemical Engineering, Medical School, Southeast University, Nanjing 211189, China.*

[b] *School of Energy and Environment, Southeast University, Nanjing 210096, China.*

[c] *Wuxi Institute of Inspection, Testing and Certification, Wuxi 214125, China.*

Experimental section

Materials

Formate dehydrogenase from *C. boidinii* (E-FDHCB, EC 1.2.1.2) was purchased from Shanghai Chaoyan Biotechnology Co., Ltd. Cadmium acetate ($C_4H_6CdO_4 \cdot 2H_2O$), thiourea, titanium butoxide, glutaraldehyde, 2-bromoethylamine hydrobromide, aniline, n-hexane, pentafluorobenzyl bromide (BM-PFB), bisphenol A (BPA), congo red (CR) and Aflatoxin B_2 (AFB_2) were purchased from Aladdin (Shanghai, China). Rhodamine 123 was obtained from KeyGEN Biotech (Nanjing, China). Phytic acid was obtained from Beijing Solarbio Science & Technology Co., Ltd. Tris-HCl buffer solution (0.05 M) was obtained from Beijing LABLEAD Inc. Pyruvic Acid (PA) Content Assay Kit was from Beijing Boxbio Science & Technology Co., Ltd. PBS was purchased from Sunncell. Chlortetracycline was from Chemleader Biomedical Co., Ltd. (Shanghai, China). NAD+/NADH Colorimetric Assay Kit was from Elabscience®Biotechnology Co., Ltd. All chemicals were used without further purification. Deionized water was prepared using a Milli-Q purification system with a resistivity of 18.2 MΩ.

Instrument

^{1}H-NMR spectra were collected from a Bruker 600 MHz spectrometer (Bruker, German). Absorbance measurement was performed through using a 2450 UV-visible spectrophotometer (Agilent, USA). Fluorescence (FL) spectra were carried out on a FluoroMax-4 spectrofluorometer with xenon discharge lamp excitation (HORIBA, USA). The morphology of CdS was characterized using scanning electron microscopy (SEM, FEI Inspect F50, America) and corresponding EDX elemental mapping images were obtained by using a JEOL model JEM 2100 (Japan). The morphology of TiO_2@CdS was characterized using high resolution transmission electron microscopy (HRTEM, Talos F200X, America) and corresponding EDX elemental mapping images were obtained by using a JEOL model JEM 2100 (Japan). X-ray diffraction (XRD) patterns of TiO_2, CdS and TiO_2@CdS were recorded by Ultima IV. X-ray photoelectron spectroscopy was carried out with Thermo ESCALAB 250XI, performed with Al Kα radiation (λ = 0.8339 nm). ICP-OES was performed with Agilent 725 (USA). The Electron Paramagnetic Resonance (EPR) measurement was performed on a Bruker A300 system at room temperature. Total organic carbon (TOC) was recorded by TOC-L. The concentration of the BPA and formate were detected by a high-performance liquid chromatography (HPLC, Agilent, USA) equipped with an X Bridge column (4.6 x 250 mm, C18, 5 mm) and an UV detector. Electrochemical impedance spectroscopy (EIS, Gamry) analysis was performed in the frequency range of 105 to 0.1 Hz at a bias potential of 0 V versus Ag/AgCl. All electrochemical experiments were performed with CHI 660B.For photocurrent-time (I-T) experiments, ITO glass was cut into 4 cm × 6 cm pieces. A 0.5 mg of TiO_2, CdS and TiO_2@CdS were mixed with 100 μL of Nafion solution (1% Nafion in CH_3CH_2OH/distilled water = 8/2) and drop-casted on the exposed area (2.65 cm × 2.65 cm) of the ITO electrode, respectively. The resulting electrode was air-dried and used as working electrode for electrochemical measurements.

Fig. S1 Schematic diagram of TiO_2@CdS (a) and FDH/DA/PANi/CC (b) synthesis.

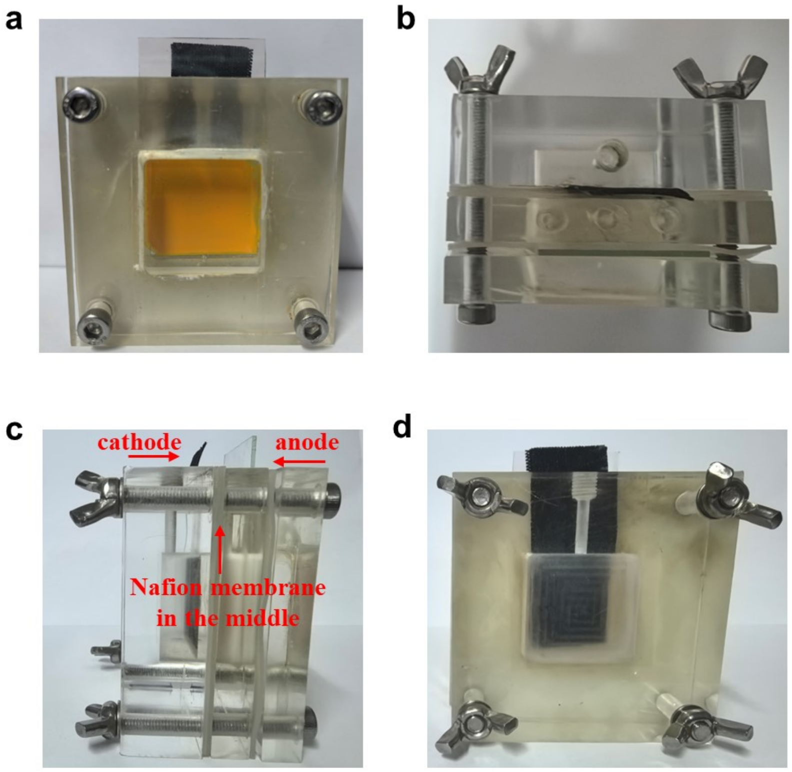

Fig. S2 Front (a), TOP (b), side (c) and back (d) view picture of PFC system.

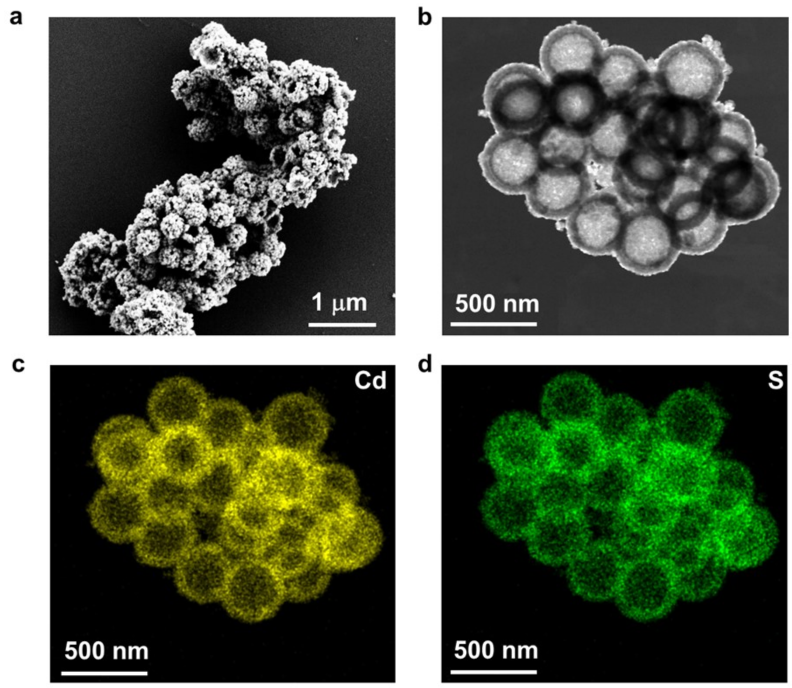

Fig. S3 SEM (a) and TEM (b) image of CdS and corresponding TEM-EDS elemental mapping images of Cd and S (c and d).

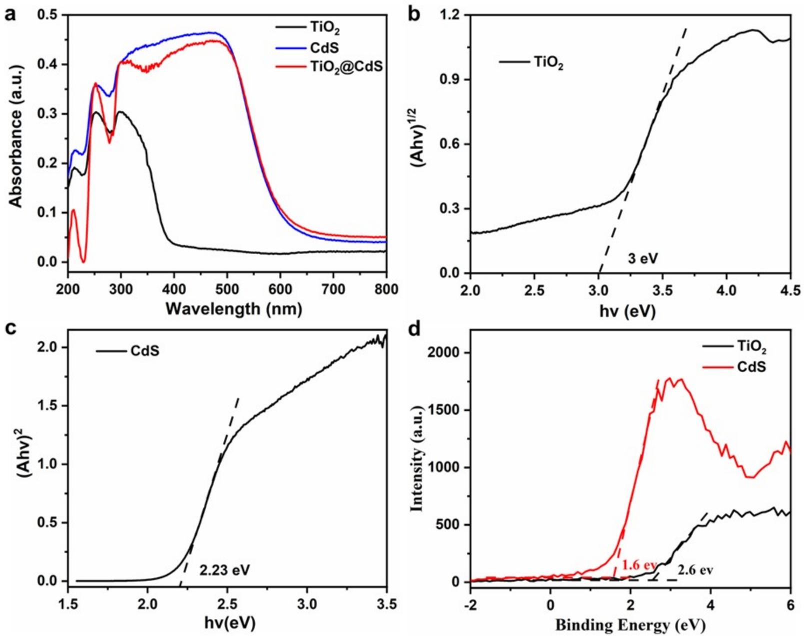

Fig. S4 (a) UV-vis diffuse reflection spectra of TiO_2, CdS and TiO_2@CdS; Bandgap of TiO_2 (b) and CdS (c) estimated from the Kubelka–Munk equation according to UV-vis diffuse reflection spectra; (d) Valence band obtained from XPS.

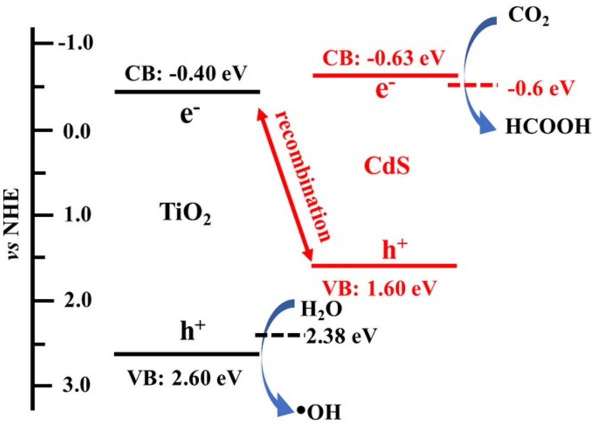

Fig. S5 The band spectrum of TiO_2@CdS heterostructures for H_2O oxidated to ·OH and CO_2 reduced to HCOOH.

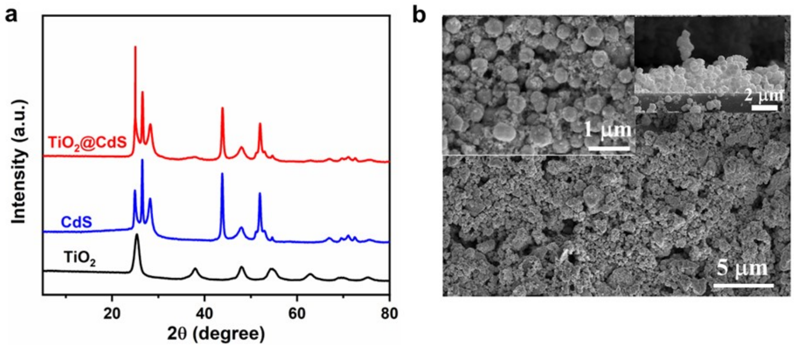

Fig. S6 (a) PXRD patterns of TiO_2, CdS and TiO_2@CdS; (b) SEM image of TiO_2@CdS/ITO (inset: the left one is a partially enlarged SEM image and the right one is the cross-sectional SEM image of TiO_2@CdS/ITO).

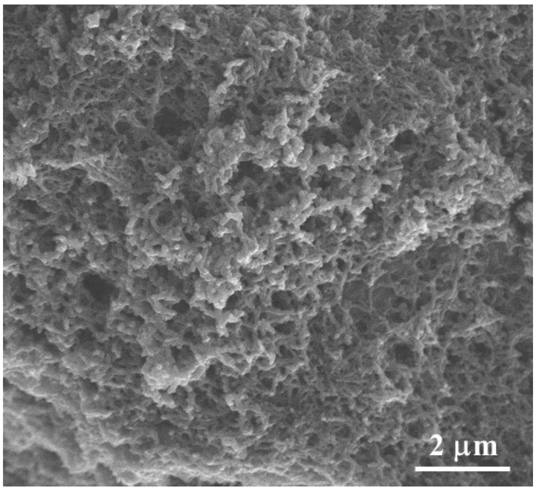

Fig. S7 SEM image of PANi/CC electrode.

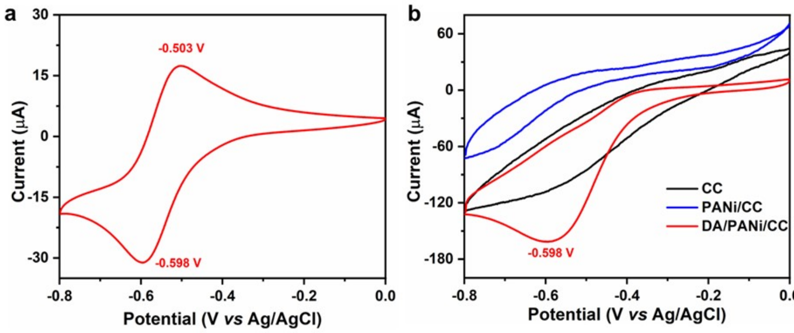

Fig. S8 (a) Cycle voltammetry curve of DA; (b) Cycle voltammetry curve of CC, PANi/CC and DA/PANi/CC.

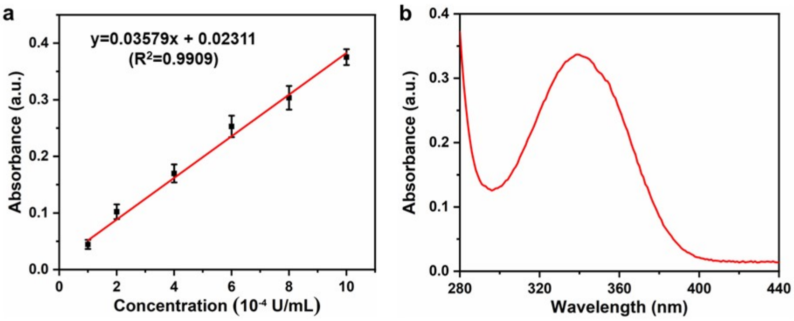

Fig. S9 (a) Standard curve of UV-vis absorbance of NADH versus concentration of FDH; (b) UV-vis absorbance of NADH of FDH/DA/PANi/CC after repeatedly washing with PBS.

After cross-linking FDH with DA/PANi/CC for 4 hours, the electrode was thoroughly washed with PBS, and the washing solutions were collected. Then, 0.1 mL of above collected solution was incubated with NAD^+ at 37 °C for 10 min. The absorption of NADH was measured by UV-vis (Fig. S9b), which could be transformed to concertation of free NADH trough the linear equation (Fig. S9a).

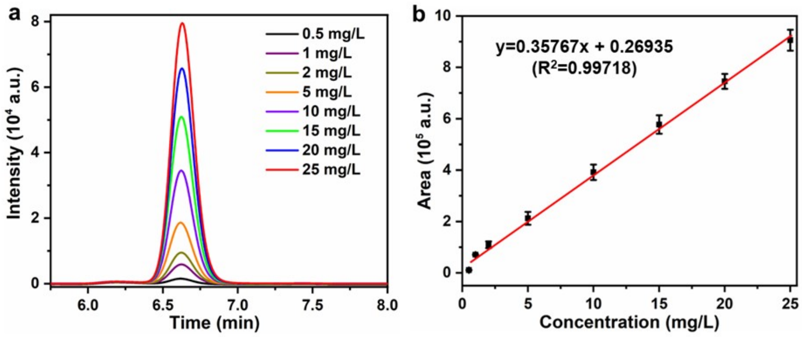

Fig. S10 (a) Curve of intensity of BPA versus its concentration; (b) Standard curve of peak area of BPA measured by HPLC versus its concentration.

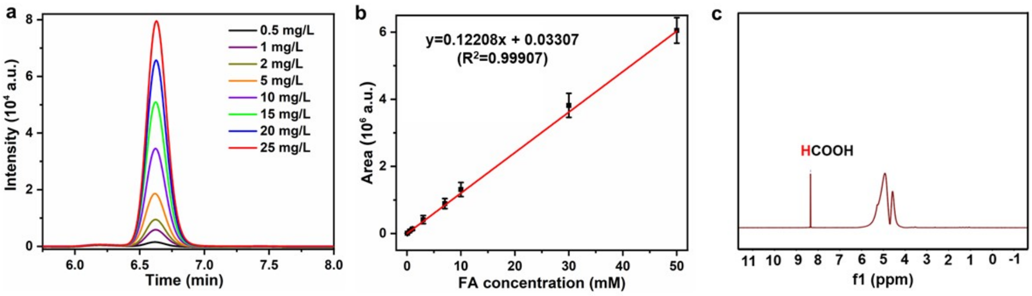

Fig. S11 (a) Curve of intensity of HCOOH versus its concentration; (b) Standard curve of peak area of HCOOH measured by HPLC versus its concentration; (c) ^{1}H-NMR spectrum of the solution after photocatalysis (400 μL solution + 100 μL D_2O).

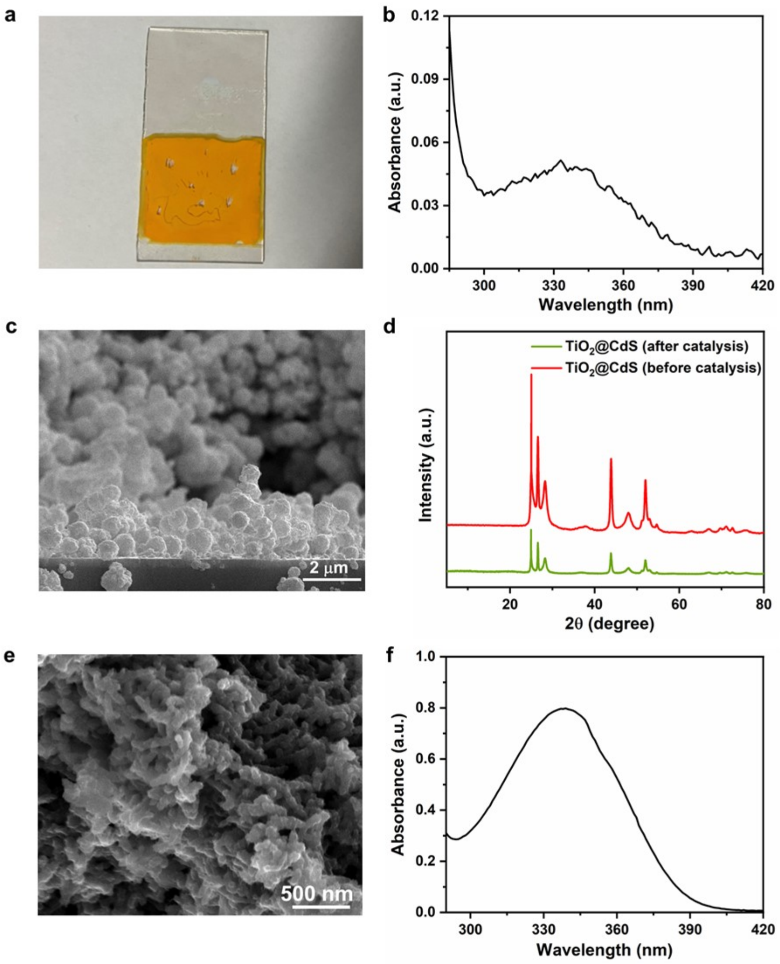

Fig. S12 (a) The image of TiO_2@CdS photoanode after photocatalytic experiment; (b) The detection of FDH of the cathode solution after photocatalytic experiment by regeneration of NADH; (c) SEM image of anode of the PFC after the 16th cycle of catalysis; (d) XRD pattern spectrum of TiO_2@CdS after the 16th cycle of catalysis; (d) SEM image of cathode of the PFC after the 16th cycle of catalysis; (f) The detection of FDH of FDH/DA/PANi/CC cathode after photocatalytic experiment by regeneration of NADH.

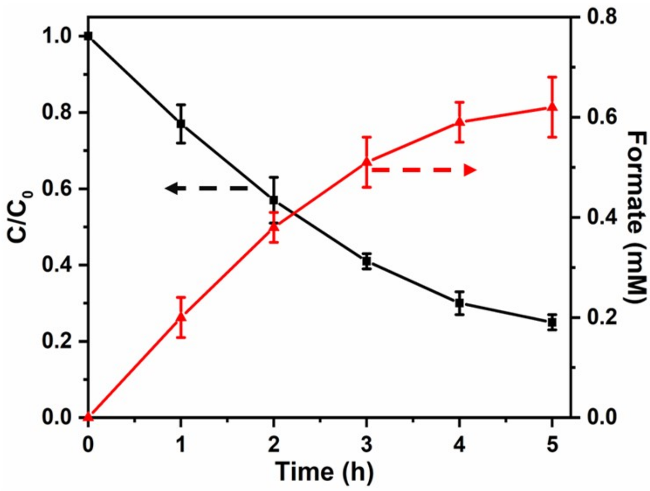

Fig. S13 The BPA degradation rate and formate production rate in the PFC system driven by the natural sunlight.

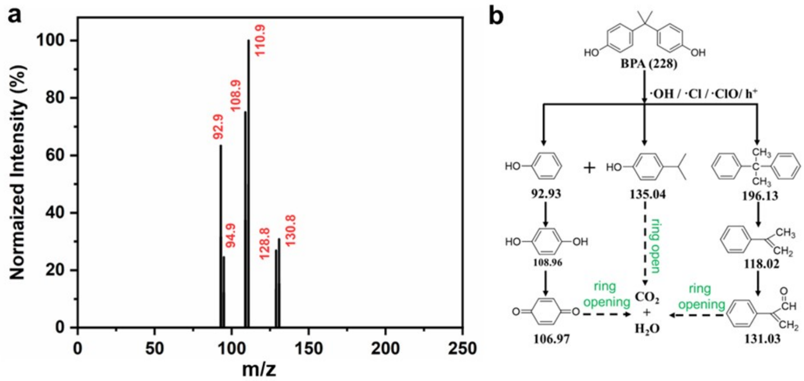

Fig. S14 (a) LC-MS spectra and proposed byproducts structure of BPA degradation after 3 h PFC reaction; (b) The proposed schematic pathway of BPA degradation via a PFC process.

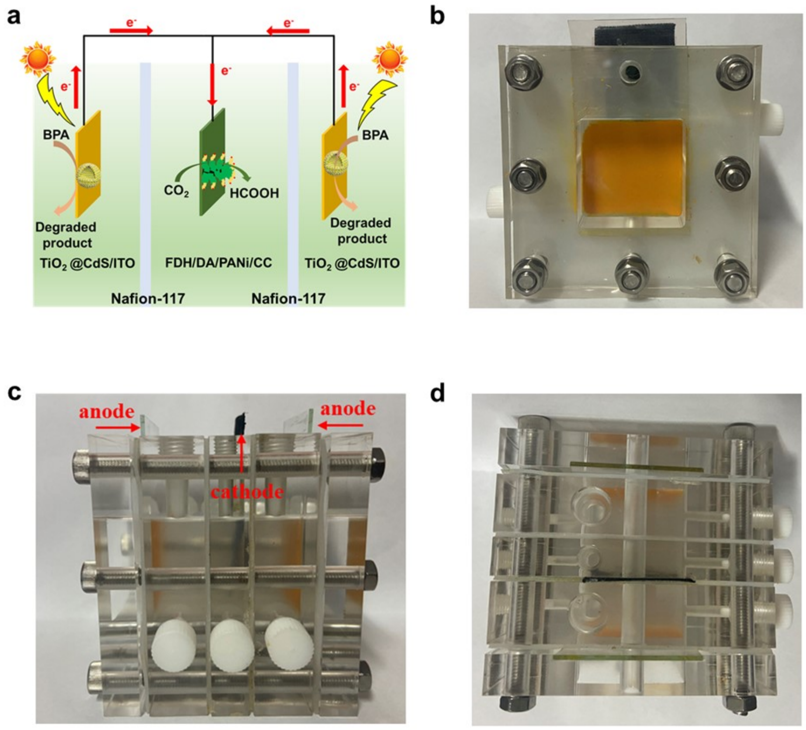

Fig. S15 (a) Schematic illustration of the 2-PFC system for BPA degradation and CO_2 reduction; Front (b), side (c) and TOP (d) view picture of 2-PFC system.

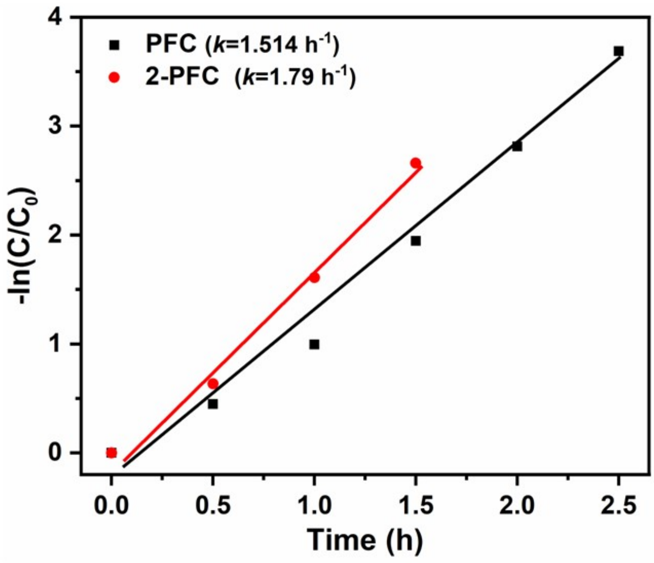

Fig. S16 Plots of -ln (C/C_0) versus time for the BPA degradation by PFC and 2-PFC systems.

Table S1 Comparison of the performance of CO_2 reduction.

Anode	Cathode	Catalyst	Electron mediator	Productivity (μmol·U^{-1}·h^{-1})	Ref
FeOOH/BiVO4/FTO	3D TiN-ClFDH	ClFDH	-	1.56	1
TiO_2/FTO	CFP	FDH	MV	0.0192	2
FeOOH-$BiVO_4$	ClFDH–TiO_2-CFO	ClFDH	-	0.098	3
FTO|IO-TiO_2|dpp|POs-PSII	FTO|IO-TiO_2|FDH	FDH	-	0.0925	4
TK/TiO_2	FDH-$CH_3V(CH_2)_9COOH$	FDH	MV derivative	0.0025	5
Ta_3N_5 NTs	g-C_3N_4	FDH	NAD^+	0.1225	6
FeOOH/$BiVO_4$	FDH/ITO	FDH	NAD^+	0.0078	7
SnTPyP/SnO_2	RuCAT-RuC$_2$-*PolyPyr*-PRu/NiO	-	-	0.062 μmol·h^{-1}	8
CoOx/$BiVO_4$	NiO/PRu-PolyPyr-RuC$_2$RuCAT$_1$	-	-	0.34 μmol·h^{-1} (-0.7 V *vs* Ag/AgCl)	9
TiO_2@CdS/ITO	FDH/DA/PANi/CC	FDH	DA	0.74 (3.88 μmol·h^{-1})	Our work
TiO_2@CdS/ITO (two)	FDH/DA/PANi/CC	FDH	DA	1.36 (7.13 μmol·h^{-1})	Our work

Table S2 Performance comparison of different PFC systems.

Anode	Cathode	Organic compound	Degradation rate (%)	V_{OC} (V)	J_{sc} (mA cm^{-2})	P_{max} (μW· cm^{-2})	Ref.
Fe@MoS_2	Carbon fiber clothe	Berberine	92.8	0.325	0.01481	0.8	10
Carbon felt	g-FeOOH	Ametryn	98.7	0.31	-	44.6	11
3DP graphene-TiO_2 aerogel	CNT/PVDF film	Phenol	96	-	0.63	110	12
GDH/SA-TCPP/TiO_2	CoNOC/BP	Phenol	100	0.83	0.87	296.9	13
TiO_2/ Ti	Cu_2O/Cu	Volatile organic compounds	22.6	0.41	0.1	20	14
WO_3	Cu_2O	chlorophenol	96.8	0.65	0.34	120	15
CN-WO_3/W	Pt	PFOA	95	0.47	0.27	17	16
g-C_3N_4/BiOI/Ti	Cu_2O/Cu	RhB	95.39	0.55	0.62	103.8	17
TiO_2@CdS/ITO	FDH/DA/PANi/CC	BPA	99.9	0.64	0.3792	94.1	Our work
TiO_2@CdS/ITO (two)	FDH/DA/PANi/CC	BPA	99.9	0.74	1.3616	186.3	Our work

Table S3 Photoluminescence quantum yield (PLQY) of TiO_2, CdS and TiO_2@CdS.

Experimental group	TiO_2	CdS	TiO_2@CdS
PLQY (%)	0.31	5.61	2.10

Table S4 Fitting parameters of PL decay curves for TiO_2, CdS and TiO_2@CdS.

Sample	τ_1 (ns)	$1/\tau_1$ (ns^{-1})	τ_2 (ns)	τ_2/τ_1	τ/ns
TiO_2	0.0042	238	0.28	66.64	0.28
CdS	22.33	0.045	70.24	3.16	0.78
TiO2@CdS	20.22	0.05	150.77	7.54	1.71

Supplemented note 1

The related equations for the generation of active species are shown as following:

$h^+ + H_2O \rightarrow \cdot OH + H^+$
$h+ + Cl- \rightarrow \cdot Cl$
$\cdot Cl + \cdot Cl \rightarrow Cl_2$
$Cl_2 + H_2O \rightarrow HClO + HCl$
$\cdot OH + HClO \rightarrow \cdot ClO + H_2O$
$\cdot Cl + HClO \rightarrow \cdot ClO + Cl^-$

References

1 S.K. Kuk, Y. Ham, K. Gopinath, P. Boonmongkolras, Y. Lee, Y.W. Lee, S. Kondaveeti, C. Ahn, B. Shin, J.K. Lee, S. Jeon, C.B. Park, *Adv. Energy Mater.*, 2019, **9**, 1900029.

2 T. Ishibashi, M. Higashi, S. Ikeda, Y. Amao, *ChemCatChem.*, 2019, **11**, 6227-6235.

3 S.K. Kuk, J. Jang, J. Kim, Y. Lee, Y.S. Kim, B. Koo, Y.W. Lee, J.W. Ko, B. Shin, J.K. Lee, C.B. Park, *ChemCatChem.*, 2020, **13**, 2940-2944.

4 K.P. Sokol, W.E. Robinson, A.R. Oliveira, J. Warnan, M.M. Nowaczyk, A. Ruff, I.A.C. Pereira, E. Reisner, *J. Am. Chem. Soc.*, 2018, **140**, 116418-16422.

5 Y. Amao, M. Fujimura, M. Miyazaki, A. Tadokoro, M. Nakamura, N. Shuto, *New J. Chem.*, 2018, **42**, 9269-9280.

6 K.Q. Xu, A. Chatzitakis, P.H. Backe, Q.S. Ruan, J.W. Tang, F. Rise, M. Bjoras, T. Norby, *Appl. Catal. B: Environ.*, 2021, **296**, 120349.

7 J. Kim, Y.W. Lee, E. Choi, P. Boonmongkolars, B.W. Jeon, H. Lee, S.T. Kim, S.K. Kuk, Y.H. Kim, B. Shin, C.B. Park, *J. Mater. Chem. A*, 2020, **8**, 88496-8502.

8 F. Kuttassery, Y. Ohsaki, A. Thomas, R. Kamata, Y. Ebato, H. Kumagai, R. Nakazato, A. Sebastian, S. Mathew, H. Tachibana, O. Ishitani, H. Inoue, *Angew. Chem. Int. Ed.,* 2023, **62**, e202308956.

9 F. Kuttassery, H. Kumagai, R. Kamata, Y. Ebato, M. Higashi, H. Suzuki, R. Abe, O. Ishitani, *Chem. Sci.*, 2021, **12**, 13216-13232.

10 L. Xu, L.F. Liu, *Appl. Catal. B: Environ.*, 2022, **304**, 120953.

11 L. Cai, H.M. Zhang, B. Dong, J. Du, Y. Tian, F. Zhang, *J. Hazard. Mater.*, 2023, **448**, 130980.

12 C.J. Zhang, X.Y. Qiao, Y.H. You, Z. He, Y.F. Wang, P. Li, Y.Y. Zhang, H.L. Fu, Z.P. Yang, *Chem. Eng. J.*, 2024, **490**, 151480.

13 J. Ding, J.G. Zhao, H. Zhang, S.J. Dong, *Biosens. Bioelectron.*, 2024, **266**, 116714.

14 C.Y. Wang, Y.X. Liu, R. Chen, X. Zhu, D.D. Ye, Y. Yang, Q. Liao, *J. Hazard. Mater.*, 2023, **447**, 130769.

15 X.F. Liu, S.J. You, N.Q. Ren, H. Zhou, J.N. Zhang, *J. Hazard. Mater.*, 2021, **416**, 11125682.

16 D. Zhang, W.J. Zhang, J.J. Zhang, L.M. Dong, X.P. Chen, Y.H. Guan, Z.N. Wang, Y.M. Li, *Chem. Eng. J.*, 2024, **480**, 147910.

17 Y.D. Zeng, Y.L. Xu, D.J. Zhong, H.Y. Yao, N.B. Zhong, *J. Hazard. Mater.*, 2022, **425**, 127967.